Geochemical Perspectives Letters

High Latitude Controls on Dissolved Barium Isotope Distributions in the Global Ocean

Y. Yu, R.C. Xie, M. Gutjahr, G. Laukert, Z. Cao, E.C. Hathorne, C. Siebert, G. Patton, M. Frank

Supplementary Information

The Supplementary Information includes:

- Sample Collection and Preparation
- Hydrography
- Laboratory Analyses and Results
- Regeneration Model
- Conservative Mixing Model
- Estimation of the Net Accumulated δ^{138}Ba Signal in the North Pacific
- Supplementary Table S-1
- Supplementary Figures S-1 to S-3
- Supplementary Information References

Sample Collection and Preparation

The seawater samples analysed in this study were collected from the Fram Strait (Nordic Seas), the Labrador Sea, the Weddell Sea, and the Pacific Ocean. The Fram Strait seawater samples were acquired along the 78.8 °N meridional transect during expedition PS80 of the German research vessel RV *Polarstern* between 15 June and 15 July 2012 (Beszczynska-Möller and Wisotzki, 2012). For Ba concentration and isotope measurements, aliquots of the filtered (0.45 µm, filtration with Millipore® cellulose acetate filters) and acidified (pH ≈ 2, on board acidification with concentrated distilled HCl) samples were selected from four full water column stations down to a maximum depth of 2668 m. More information on sample collection, hydrography and CTD (conductivity, temperature, depth) profiles are available from Laukert *et al.* (2017). Aliquots of filtered (0.2 µm, direct filtration with PALL filters) and acidified (same pH and procedure as for the Fram Strait samples) seawater samples from the Labrador Sea were chosen from four stations conducted during the cruise MSM39 and the cruise MSM45 PULSE (Paleoclimate Understanding Labrador Sea) of the German research vessel RV *Maria S. Merian* in June 2014 and August 2015 (Schneider *et al.*, 2016). Aliquots of the Weddell Sea samples (filtered and acidified in the same manner as the Labrador Sea samples) were picked from four full depth profiles in the southern and western Weddell Sea during the two expeditions PS111 and PS118 of the German research vessel RV *Polarstern* in 2018 and 2019. Further details on sampling and hydrographic conditions are available from the cruise reports of PS111 and PS118 (Schröder, 2018; Dorschel, 2019). Aliquots of the Pacific samples (filtered

and acidified in the same manner as the Labrador Sea samples) were picked from five depth profiles in the South and North Pacific during the expedition SO264 of the German research vessel RV *Sonne* in 2018 (Nürnberg, 2018). More information on sample collection, hydrography and CTD (conductivity, temperature, depth) profiles are available from Fuhr *et al.* (2021).

Hydrography

Figure S-1 provides a *T*-*S* diagram for all deep water masses encountered in this study contoured by potential density. The measured Ba concentrations ([Ba]) and isotope compositions (δ^{138}Ba) for all water samples are presented in Table S-1 with their hydrographic properties and water masses. In the Nordic Seas, the East Greenland Current (EGC) transports cold and fresh shallow waters exiting the Arctic Ocean and Atlantic Water (AW) recirculating in the Fram Strait or in the Arctic Ocean across the Greenland Scotland Ridge (GSR) forming a part of the Nordic Seas overflows (Dickson *et al.*, 1990). Once the Northern Overflow Water (NOW) has crossed the GSR as the Denmark Strait Overflow Water (DSOW) and the Iceland Scotland Overflow Water (ISOW), they descend and subsequently entrain intermediate waters present in the Irminger and Iceland Basins, such as Labrador Sea Water (LSW) and Subpolar Mode Water (SPMW). This process forms Northwest Atlantic Bottom Water (NWABW) and Northeast Atlantic Deep Water (NEADW; Dickson and Brown, 1994). Thereafter, NWABW and NEADW merge south of the Denmark Strait forming the upper and lower branches of the Deep Western Boundary Current (DWBC) when reaching Cape Farewell. The DWBC subsequently flows into the Labrador Basin and mixes with LSW thereby forming North Atlantic Deep Water (NADW), which constitutes the northern-deep limb of the Atlantic meridional overturning circulation (AMOC; Dickson and Brown, 1994; Yashayaev, 2007). In the Southern Ocean, the circulation regime is dominated by the eastward flowing Antarctic Circumpolar Current (ACC) and the cyclonically circulating Weddell Gyre (WG) that is located between the southern boundary of the ACC and the Antarctic shelf of the Weddell Sea (Fahrbach *et al.*, 1994). The two major source waters that contribute to the formation of Antarctic Bottom Water (AABW) are warm remnants of the regional Circumpolar Deep Water (CDW) that have been imported from the ACC, and the extremely cold and dense shelf waters resulting from brine rejection during sea-ice formation (Orsi *et al.*, 1999). Part of this mixture that is dense enough to reach the bottom forms Weddell Sea Bottom Water (WSBW), which is, however, too dense to escape from the Weddell Basin (Stichel *et al.*, 2012). Only the less dense part of the mixture can feed into Weddell Sea Deep Water (WSDW), which leaves the Weddell Basin via deep gaps across the South Scotia Ridge and becomes the major contributor to AABW constituting the southern-deep limb of the AMOC (Orsi *et al.*, 1999). The deep-water circulation in the North Pacific is mainly driven by density gradients and is characterised by the advection and mixing of Lower and Upper Circumpolar Deep Water (LCDW/UCDW) and North Pacific Deep Water (NPDW). The UCDW initially follows the Antarctic Intermediate Water (AAIW) at greater depths but takes a more north-westerly path into the Caroline Basin and further into the Philippine Sea where it eventually upwells (Kawabe and Fujio, 2010).

Laboratory Analyses and Results

The dissolved seawater Ba concentrations ([Ba]) were analysed applying an isotope dilution technique with an Agilent 7500ce inductively coupled plasma mass spectrometer (ICP-MS) at GEOMAR, Kiel. Briefly, an aliquot (50 µL) of acidified seawater was accurately weighed and mixed with defined amounts of an ^{135}Ba single spike to achieve a ^{138}Ba/^{135}Ba ratio near 0.64. The spike-equilibrated samples were then diluted to about 500 µL with 2 % HNO_3 before the ^{138}Ba/^{135}Ba ratios were measured and mass bias corrected by bracketing analyses of a natural Ba standard solution. Depending on Ba concentration, aliquots of 5 mL (>60 nmol kg^{-1}) or 10 mL (<60 nmol kg^{-1}) of the seawater samples were appropriately spiked with an ^{130}Ba-^{135}Ba double spike. After an equilibration period of 24 hours, Ba was co-precipitated with $CaCO_3$ and the resulting precipitates were centrifuged and dissolved in 2 mL of 1 M HCl in preparation

for cation exchange chromatography. Samples were twice passed through columns containing 1.4 mL of Bio-Rad AG 50W-X8 (200–400 mesh size) resin. Matrix elements were subsequently eluted with 8 mL of 1 M HCl and 8 mL of 3 M HCl, respectively. The Ba cuts were then collected with 10 mL of 2 M HNO_3, dried and re-dissolved in 2 % (v/v) HNO_3 for Ba isotope analyses. Stable Ba isotope measurements were performed with a Thermo Fisher Neptune Plus MC-ICP-MS at GEOMAR, Kiel. The analyte was introduced as a dry aerosol using an Aridus II desolvating system (CETAC Technologies, Omaha, NE, USA) and an Aspire PFA micro-concentric nebuliser (uptake rate of ~ 50 µL min^{-1}). The MC-ICP-MS was tuned to a matrix tolerance state defined by a high Normalised Argon Index value (NAI, an index of plasma temperature; Yu *et al.* 2020). A three-dimensional data reduction procedure following Siebert *et al.* (2001) was used to correct for both instrumental and natural mass-dependent isotope fractionation. The Ba isotope compositions are reported in per mil (‰) relative to the National Institute of Standards and Technology (NIST) SRM 3014a Ba standard ($\delta^{138}Ba = {}^{138/134}Ba_{sample}/{}^{138/134}Ba_{NIST} - 1$). The uncertainty is reported as the larger of either the internal 2 standard error (2 s.e.) of repeated sample measurements or the long-term 2 s.d. reproducibility (±0.04 ‰) of repeated SAFe 1000 m measurements.

The depth profiles of [Ba] and $\delta^{138}Ba$ are shown in Figure S-2. In the Fram Strait, the depth profiles of [Ba] and $\delta^{138}Ba$ are similar for all four stations in that Ba is modestly depleted in surface waters associated with relatively heavy $\delta^{138}Ba$ values of 0.52 ‰. With increasing depth from 200 m to the bottom, [Ba] generally increases from 43 to 49 nmol kg^{-1} and $\delta^{138}Ba$ values slightly decrease from 0.52 to 0.46 ‰. In the Labrador Sea, the vertical distributions of $\delta^{138}Ba$ and [Ba] are similar to those of the Fram Strait and only display little variability along the cyclonic circulation within the Labrador Basin. Dissolved [Ba] exhibits moderate depletion at the surface and relative enrichment at depth, resembling nutrient-type depth profiles and mirroring the $\delta^{138}Ba$ profiles. All depth profile samples below 1000 m water depth, where NADW dominates (Dickson and Brown, 1994), feature an average $\delta^{138}Ba$ value of 0.48 ‰ and an average [Ba] value of 50 nmol kg^{-1}. In the Weddell Sea, the depth profiles show slight enrichments towards heavy isotopic compositions in the surface layer relative to deeper waters, which are associated with lower [Ba] values. The nature of the vertical gradient in $\delta^{138}Ba$ and its relationship to [Ba] varies insignificantly with sampling sites along the WG, as well as with water depth. Such a vertical distribution is also consistent with the pattern reported for St. Super5 at the north rim of the WG (Fig. S-2; Hsieh and Henderson, 2017). At depths between 2000 and 4000 m, where the water masses are dominated by WSDW/AABW (Orsi *et al.*, 1999), dissolved [Ba] and $\delta^{138}Ba$ are constrained to average values of 99 nmol kg^{-1} and 0.26 ‰, respectively. In the Pacific Ocean, surface and sub-surface waters are characterised by higher $\delta^{138}Ba$ values than those from the Atlantic Ocean. The deep-water masses (below 2000 m) are characterised by Ba isotope compositions indistinguishable from those of the deep Weddell Sea but significantly higher [Ba]. In the tropical South Pacific, LCDW exhibits a $\delta^{138}Ba$ value of 0.28 ‰ and a [Ba] value of 120 nmol kg^{-1}, while NPDW is characterised by a $\delta^{138}Ba$ value of 0.25 ‰ and a [Ba] value of 160 nmol kg^{-1} in the high-latitude North Pacific.

Regeneration Model

A regeneration model has been applied to explain the relationship between dissolved $\delta^{138}Ba$ and [Ba] in seawater samples. Based on isotope mass balance, the continuous addition of Ba to deep waters by dissolution of sinking particles causes systematic changes in $\delta^{138}Ba$ and [Ba]. In this case, the following equation can be applied following the method from Bridgestock *et al.* (2018):

$$\delta^{138}Ba = (\delta^{138}Ba_{pre} \times f_{pre}) + (\delta^{138}Ba_{regen} \times f_{regen}), \quad \text{(Eq. S-1)}$$

where $\delta^{138}Ba_{pre}$ and $\delta^{138}Ba_{regen}$ denote the Ba isotope composition of the preformed and the regenerated fractions, respectively. f_{pre} and f_{regen} denote the fraction of the Ba from the preformed and regenerated reservoirs, respectively ($f_{pre} + f_{regen} = 1$). If there is no isotope fractionation accompanying Ba regeneration, this model assumes that increases in [Ba] and associated decreases in $\delta^{138}Ba$ with depth are purely controlled by the addition of Ba from sinking particles.

Assuming [Ba] and δ^{138}Ba value of 35 nmol kg^{-1} and 0.62 ‰ represents the preformed signals with a characterised sinking particles δ^{138}Ba value of 0.10 ‰ (Horner *et al.*, 2017; Bridgestock *et al.*, 2018), the regeneration model defines a linear correlation in a plot of δ^{138}Ba against 1/[Ba], which gradually deviates from the mixing relationship at higher [Ba] (Fig. 4).

Conservative Mixing Model

A conservative mixing model has been applied by using salinity (S) as a conservative tracer to quantify the variability of dissolved Ba isotopes (δ^{138}Ba) not related to conservative mixing in the low and mid-latitude Atlantic and Pacific Ocean. The conservative mixing model is described by:

$$S_{mix} = S_a \times f_a + S_b \times f_b, \quad \text{(Eq. S-2)}$$

$$\delta^{138}Ba_{mix} = ([Ba]_a \times \delta^{138}Ba_a \times f_a + [Ba]_b \times \delta^{138}Ba_b \times f_b) / ([Ba]_a \times f_a + [Ba]_b \times f_b), \quad \text{(Eq. S-3)}$$

where mix, a and b denote the components of the mixed and a and b endmember water masses, respectively. The factors f_a and f_b denote the fractional contributions of the two endmember water masses ($f_a + f_b = 1$). For mixing calculations in the deep Atlantic, NADW (S = 35.00, δ^{138}Ba = 0.48 ‰, [Ba] = 50 nmol kg^{-1}) and AABW (S = 34.70, δ^{138}Ba = 0.26 ‰, [Ba] = 99 nmol kg^{-1}) were used as simplified water mass endmembers. For mixing calculations in the deep Pacific, LCDW (S = 34.70, δ^{138}Ba = 0.28 ‰, [Ba] = 120 nmol kg^{-1}) and NPDW (S = 34.60, δ^{138}Ba = 0.25 ‰, [Ba] = 160 nmol kg^{-1}) were used as simplified water mass endmembers. Deviations from conservative mixing exceeding 0.04 ‰ indicate non-conservative behaviour, based on the 2 s.d. uncertainty of the Ba isotope measurements carried out at GEOMAR. As shown in Figure S-3, the signatures of all water samples below 2000 m from the low and mid-latitude deep Atlantic and Pacific do not deviate from the mixing lines in both ocean basins taking into account the analytical uncertainty of the Ba isotope measurements.

Estimation of the Net Accumulated δ^{138}Ba Signal in the North Pacific

A 34 % increase in deep water [Ba] from the Southern Ocean to the North Pacific, without a corresponding variation in δ^{138}Ba, puts constraints on the Ba isotope compositions of the net accumulated dissolved Ba from remineralisation of sinking particles in the North Pacific. A simple mass balance calculation developed for stable Cd isotopes by Janssen *et al.* (2017) is applied to estimate the accumulated δ^{138}Ba signal in the North Pacific:

$$[Ba]_{SO} + [Ba]_{acm} = [Ba]_{Pac}, \quad \text{(Eq. S-4)}$$

$$[Ba]_{SO} \times \delta^{138}Ba_{SO} + [Ba]_{acm} \times \delta^{138}Ba_{acm} = [Ba]_{Pac} \times \delta^{138}Ba_{Pac}, \quad \text{(Eq. S-5)}$$

where $[Ba]_{SO}$, $[Ba]_{acm}$ and $[Ba]_{Pac}$ denote the Ba concentrations of the deep Southern Ocean, the accumulated fraction and the deep North Pacific, respectively. $\delta^{138}Ba_{SO}$, $\delta^{138}Ba_{acm}$ and $\delta^{138}Ba_{Pac}$ denote the Ba isotope compositions of the deep Southern Ocean, the accumulated fraction and the deep North Pacific, respectively. Using the arithmetic mean of deep water δ^{138}Ba from each water mass and the 2 s.d. error on this mean, the net accumulated Ba in the deep North Pacific is characterised by an average $\delta^{138}Ba_{acm}$ value of 0.22 ± 0.24 ‰.

Supplementary Table

Table S-1 Detailed data for the seawater samples from this study.

Table S-1 (.xlsx) can be downloaded from the online version of this article at https://doi.org/10.7185/geochemlet.2242.

Supplementary Figures

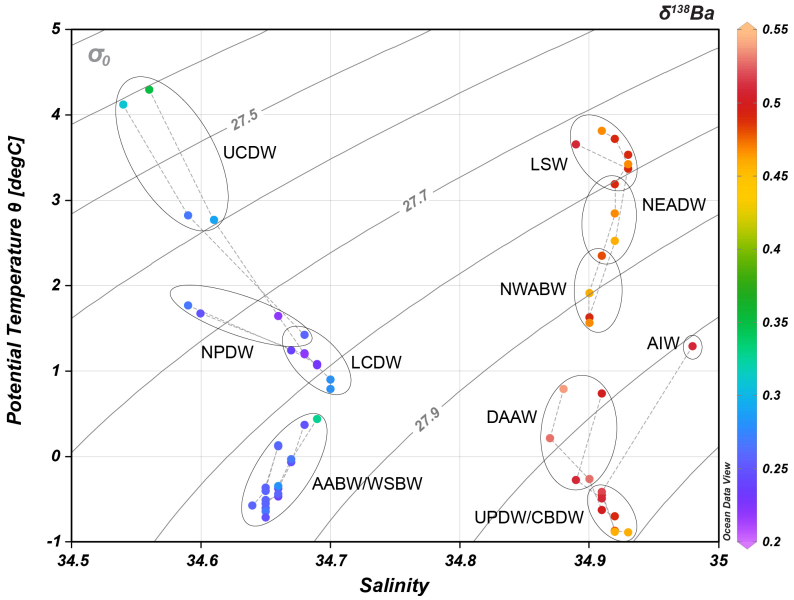

Figure S-1 *T-S* diagram for all deep water masses encountered in this study contoured by potential density. The water masses are marked with circles. Colours indicate the dissolved Ba isotope compositions (δ^{138}Ba). UCDW, Upper Circumpolar Deep Water; NPDW, North Pacific Deep Water; LCDW, Lower Circumpolar Deep Water; AABW, Antarctic Bottom Water; WSBW, Weddell Sea Bottom Water; LSW, Labrador Sea Water; NEADW, Northeast Atlantic Deep Water; NWABW, Northwest Atlantic Bottom Water; AIW, Arctic Intermediate Water; DAAW, Dense Arctic Atlantic Water; UPDW, Upper Polar Deep Water; CBDW, Canadian Basin Deep Water. Figure was produced using Ocean Data View (Schlitzer, 2022) and modified manually.

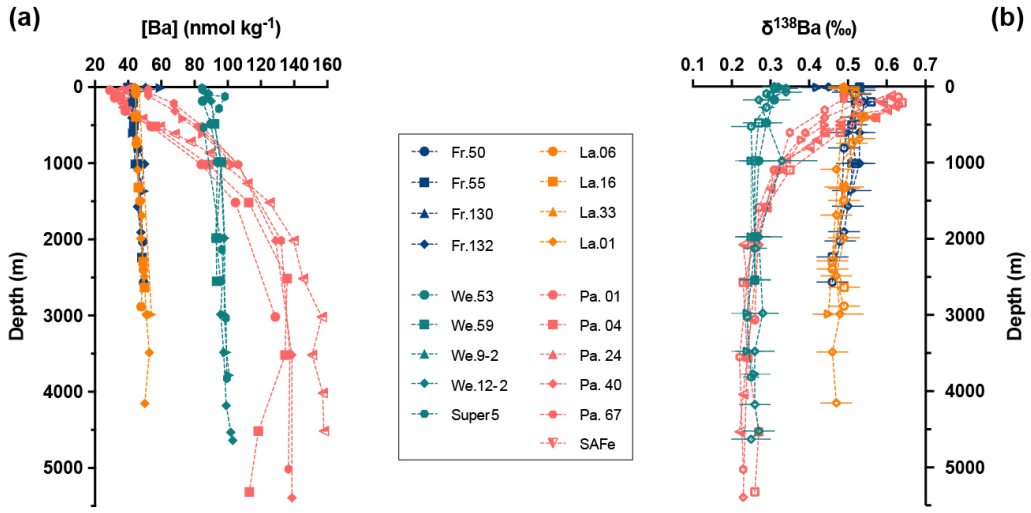

Figure S-2 Depth profiles of the **(a)** dissolved Ba concentrations and **(b)** isotope compositions in the Fram Strait (blue), the Labrador Sea (orange), the Weddell Sea (green) and the Pacific Ocean (pink). The error bars for δ^{138}Ba are the larger of either the internal 2 s.e. of repeated sample measurements or the long-term 2 s.d. reproducibility (±0.04 ‰) of repeated SAFe (1000 m) measurements. Data for station Super5 and SAFe are from Hsieh and Henderson (2017) and Geyman *et al.* (2019), respectively.

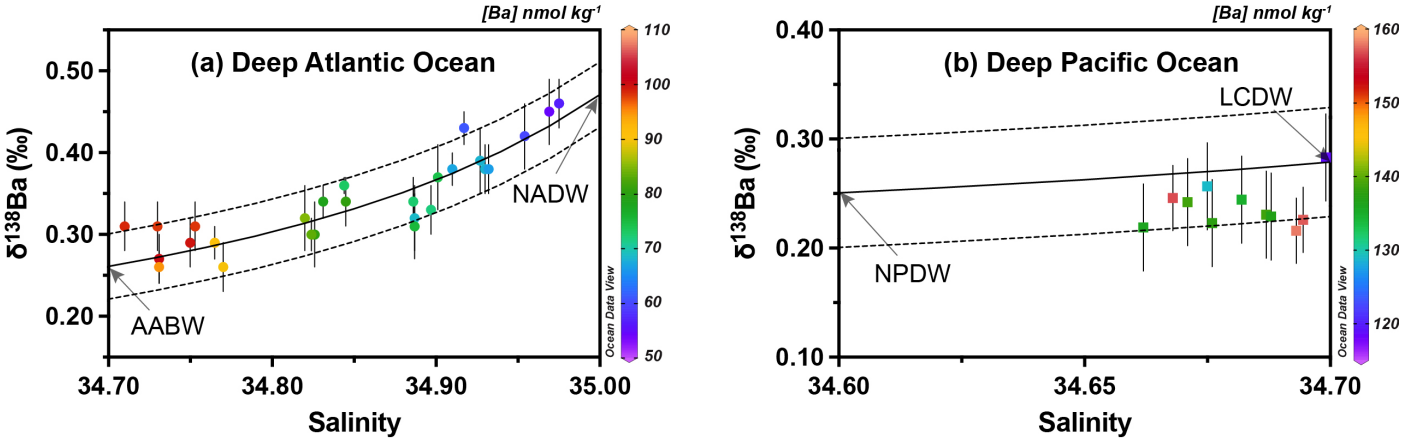

Figure S-3 Salinity *versus* δ^{138}Ba diagrams for deep water masses of the **(a)** Atlantic and **(b)** Pacific Ocean below 2000 m water depth; colours denote dissolved [Ba]. All measured δ^{138}Ba values from the low and mid-latitude oceans are consistent within analytical error with the conservative mixing curves and their 0.04 ‰ uncertainty range (dashed curves). NADW, North Atlantic Deep Water; AABW, Antarctic Bottom Water; LCDW, Lower Circumpolar Deep Water; NPDW, North Pacific Deep Water. Figures were produced using Ocean Data View (Schlitzer, 2022) and modified manually.

Supplementary Information References

Beszczynska-Möller, A., Wisotzki, A. (2012) *Physical oceanography during POLARSTERN cruise ARK-XXVII/1*. Alfred Wegener Institute, Helmholtz Centre for Polar and Marine Research, Bremerhaven; PANGAEA. https://doi.org/10.1594/PANGAEA.801791

Bridgestock, L., Hsieh, Y.-T., Porcelli, D., Homoky, W.B., Bryan, A., Henderson, G.M. (2018) Controls on the barium isotope compositions of marine sediments. *Earth and Planetary Science Letters* 481, 101–110. https://doi.org/10.1016/j.epsl.2017.10.019

Dickson, R.R., Brown, J. (1994) The production of North Atlantic Deep Water: Sources, rates, and pathways. *Journal of Geophysical Research: Oceans* 99, 12319–12341. https://doi.org/10.1029/94JC00530

Dickson, R.R., Gmitrowicz, E.M., Watson, A.J. (1990) Deep-water renewal in the northern North Atlantic. *Nature* 344, 848–850. https://doi.org/10.1038/344848a0

Dorschel, B. (2019) The Expedition PS118 of the Research Vessel POLARSTERN to the Weddell Sea in 2019. *Reports on Polar and Marine Research* 735, Alfred-Wegener-Institut, Helmholtz-Zentrum für Polar- und Meeresforschung, Bremerhaven, Germany, 149 pp. https://doi.org/10.2312/BzPM_0735_2019

Fahrbach, E., Rohardt, G., Schröder, M., Strass, V. (1994) Transport and structure of the Weddell Gyre. *Annales Geophysicae* 12, 840–855. https://doi.org/10.1007/s00585-994-0840-7

Fuhr, M., Laukert, G., Yu, Y., Nürnberg, D., Frank, M. (2021) Tracing Water Mass Mixing from the Equatorial to the North Pacific Ocean with Dissolved Neodymium Isotopes and Concentrations. *Frontiers in Marine Science* 7, 603761. https://doi.org/10.3389/fmars.2020.603761

Geyman, B.M., Ptacek, J.L., LaVigne, M., Horner, T.J. (2019) Barium in deep-sea bamboo corals: Phase associations, barium stable isotopes, & prospects for paleoceanography. *Earth and Planetary Science Letters* 525, 115751. https://doi.org/10.1016/j.epsl.2019.115751

Horner, T.J., Pryer, H.V., Nielsen, S.G., Crockford, P.W., Gauglitz, J.M., Wing, B.A., Ricketts, R.D. (2017) Pelagic barite precipitation at micromolar ambient sulfate. *Nature Communications* 8, 1342. https://doi.org/10.1038/s41467-017-01229-5

Hsieh, Y.-T., Henderson, G.M. (2017) Barium stable isotopes in the global ocean: Tracer of Ba inputs and utilization. *Earth and Planetary Science Letters* 473, 269–278. https://doi.org/10.1016/j.epsl.2017.06.024

Janssen, D.J., Abouchami, W., Galer, S.J.G., Cullen, J.T. (2017) Fine-scale spatial and interannual cadmium isotope variability in the subarctic northeast Pacific. *Earth and Planetary Science Letters* 472, 241–252. https://doi.org/10.1016/j.epsl.2017.04.048

Kawabe, M., Fujio, S. (2010) Pacific ocean circulation based on observation. *Journal of Oceanography* 66, 389–403. https://doi.org/10.1007/s10872-010-0034-8

Laukert, G., Frank, M., Bauch, D., Hathorne, E.C., Rabe, B., von Appen, W.-J., Wegner, C., Zieringer, M., Kassens, H. (2017) Ocean circulation and freshwater pathways in the Arctic Mediterranean based on a combined Nd isotope, REE and oxygen isotope section across Fram Strait. *Geochimica et Cosmochimica Acta* 202, 285–309. https://doi.org/10.1016/j.gca.2016.12.028

Nürnberg, D. (Ed.) (2018) *RV SONNE Fahrtbericht / Cruise Report SO264-SONNE-EMPEROR: The Plio/Pleistocene to Holocene development of the pelagic North Pacific from surface to depth – assessing its role for the global carbon budget and Earth's climate, Suva (Fiji) – Yokohama (Japan), 30.6. – 24.8.2018*. GEOMAR Helmholtz-Zentrum für Ozeanforschung, Kiel, Germany, 284 pp. https://doi.org/10.3289/GEOMAR_REP_NS_46_2018

Orsi, A.H., Johnson, G.C., Bullister, J.L. (1999) Circulation, mixing, and production of Antarctic Bottom Water. *Progress in Oceanography* 43, 55–109. https://doi.org/10.1016/S0079-6611(99)00004-X

Schlitzer, R. (2022) Ocean Data View. http://odv.awi.de

Schneider, R.R., Blanz, T., Evers, F., Gasparotto, M.-C., Gross, F., Hüls, M., Keul, N., Kienast, M., Lehner, K., Lüders, S., Mellon, S., Merl, M., Reissig, S., Repschläger, J., Salvatteci, R., Schulten, I., Schwarz, J.-P., Schönke, M., Steen, E., Tietjens, A., Van Nieuwenhove, N. (2016) Paleoclimate Understanding Labrador Sea (PULSE), Cruise No. MSM45, August 1, 2015 - August 21, 2015, Nuuk (Greenland) - Halifax (Canada). *MARIA S. MERIAN-Berichte* MSM45, Gutachterpanel Forschungsschiffe, Bonn, Germany, 38 pp. https://doi.org/10.2312/cr_msm45

Schröder, M. (2018) The Expedition PS111 of the Research Vessel POLARSTERN to the southern Weddell Sea in 2018. *Reports on Polar and Marine Research* 718, Alfred-Wegener-Institut, Helmholtz-Zentrum für Polar- und Meeresforschung, Bremerhaven, Germany, 161 pp. https://doi.org/10.2312/BzPM_0718_2018

Siebert, C., Nägler, T.F., Kramers, J.D. (2001) Determination of molybdenum isotope fractionation by double-spike multicollector inductively coupled plasma mass spectrometry. *Geochemistry, Geophysics, Geosystems* 2, 2000GC000124. https://doi.org/10.1029/2000GC000124

Stichel, T., Frank, M., Rickli, J., Hathorne, E.C., Haley, B.A., Jeandel, C., Pradoux, C. (2012) Sources and input mechanisms of hafnium and neodymium in surface waters of the Atlantic sector of the Southern Ocean. *Geochimica et Cosmochimica Acta* 94, 22–37. https://doi.org/10.1016/j.gca.2012.07.005

Yashayaev, I. (2007) Hydrographic changes in the Labrador Sea, 1960–2005. *Progress in Oceanography* 73, 242–276. https://doi.org/10.1016/j.pocean.2007.04.015

Yu, Y., Siebert, C., Fietzke, J., Goepfert, T., Hathorne, E., Cao, Z., Frank, M. (2020) The impact of MC-ICP-MS plasma conditions on the accuracy and precision of stable isotope measurements evaluated for barium isotopes. *Chemical Geology* 549, 119697. https://doi.org/10.1016/j.chemgeo.2020.119697